04,08

Charge transport mechanism in forming-free MgO-based memristor

© A.A. Gismatulin[1], D.V. Gorshkov[2], E.Y. Gerasimov[3], V.A. Gritsenko[1,4]

[1] Rzhanov Institute of Semiconductor Physics, Siberian Branch, Russian Academy of Sciences,
Novosibirsk, Russia
[2] AO „Katod“,
Novosibirsk, Russia
[3] Boreskov Institute of Catalysis, Siberian Branch of RAS,
Novosibirsk, Russia
[4] Novosibirsk State Technical University,
Novosibirsk, Russia

E-mail: aagismatulin@isp.nsc.ru

Received January 26, 2026
Revised January 27, 2026
Accepted January 30, 2026

The charge transport mechanism was determined in the high-resistance and low-resistance states of a forming-free MgO-based memristor. The MgO-based memristor showed a memory window of about three orders of magnitude. It is established that the charge transport mechanism in a MgO-based memristor in the high-resistance and low-resistance states is the space-charge-limited current model. The trap parameters in the MgO-based memristor in the high-resistance ($N_t = 1.7 \cdot 10^{18}\,\mathrm{cm}^{-3}$) and low-resistance ($N_t = 0.8 \cdot 10^{18}\,\mathrm{cm}^{-3}$) states were determined.

Keywords: forming-free, memristor, space-charge-limited current, charge transport.

DOI: 10.61011/PSS.2026.01.63242.9021-25

Thin films of magnesium oxide (MgO) are intensively studied for use in various electronic devices [1,2]. MgO is also used in solar energy converters due to its high efficiency [3]. A thin layer of MgO is also used in magnetoresistive spin moment transfer RAM (STT-MRAM) [4,5]. MgO can also be used as an active medium for the memristor [6–9]. Memristors as a replacement for flash memory have several advantages: high performance (~ 100 ps), low power consumption (10 fJ), a large number of erase/write cycles (up to 10^{12} cycles), simple architecture memory cells, low cost, the ability to store information for 10 years at 85 °C, compatible with silicon technology. Compared with other metallic dielectrics such as TiO_2, Ta_2O_5, HfO_2, ZrO_2, MgO has several advantages: a large band gap (7.3–7.8 eV) [10,11], high thermal stability and high dielectric breakdown field value. (12 MV/cm) [11]. The advantage of MgO-based memristors is the low switching voltages [12]. MgO-based memristors are also used in biodegradable neuromorphic electronics [12–15].

But despite the widespread use of MgO layers in various devices, the mechanism of charge transport has not been clearly defined. In this paper, we focused on studying an MgO-based memristor and determining the mechanism of charge transport in the high resistive state (HRS) and low resistive state (LRS) states of this memristor.

The growth of the MgO layer was carried out using electron beam sputtering from MgO granules with a diameter of 1–2 mm, with a purity of 99.99 % (manufactured by Ohara GmbH, Germany). The deposition took place on a silicon substrate *p*-type with a resistance of $10\,\Omega \cdot \mathrm{cm}$. The residual pressure in the chamber during MgO spraying was no more than 10^{-3} Pa. The growth rate of MgO was 0.1 nm/s, and the thickness of MgO was 14 nm. To create the structure of metal–dielectric–semiconductor (MDS), aluminum contacts were applied to MgO through a shadow mask by thermal spraying. The lower aluminum contact was also obtained by thermal spraying over the entire area of the silicon substrate. Current-voltage (I-V) characteristics of MDS was measured using a Keithley 2400 electrometer, the voltage sweep rate was 0.9 V/s. Temperature measurements in the temperature range of 300 to 350 K were carried out in an LTS420E temperature cell controlled by a Linkam T95 controller (Linkam Scientific Instruments, Great Britain). The morphology of the samples was analyzed by scanning electron microscopy (SEM) on a Hitachi Regulus SU 8230 FE-SEM microscope (Hitachi High Technologies, Japan) with an AztecLive EDX spectrometer (Oxford Instruments, England). The microscope operated in the secondary electron mode at an accelerating voltage of 10 kV.

According to the results of scanning electron microscopy (Figure 1), it was found that the magnesium oxide film is evenly distributed over the surface of the silicon wafer. The film structure mainly consists of magnesium oxide grains with a size of 20–50 nm. In addition, morphological examination showed the presence of a small number of magnesium carbonate islands smaller than 100 μm, observed in the images as round dark particles. These particles could have formed during the transfer of the sample in the air for conducting experiments on electron microscopy. According to the energy dispersive X-ray spectroscopy (EDX) method (see the box in Figure 1), only Mg, O, Si, and C are observed.

Figure 2 shows the current-voltage characteristics of an MgO-based memristor. The voltage sweep occurred from 0 to 4 V with a current limit of 0.1 mA. The numbers *1–5* in Figure 2 show the sequence of the full cycle of switching the resistances of the memristor. The ratio of HRS to LRS at −0.5 V is about 3 orders of magnitude.

The temperature dependences of the current in HRS and LRS were obtained to determine the mechanism of charge transport. In both states, there is a weak temperature dependence of the current at low voltages, and at high voltages, the current dependence on temperature disappears.

The current in a dielectric with traps is determined by the following expression:

$$I = eN^{2/3}PS, \tag{1}$$

where e is the electron charge, N is the trap concentration. P — probability of trap ionization, S — area involved in charge transport.

The Frenkel effect consists in lowering the ionization energy of the Coulomb trap in the electric field [16,17]. The probability of ionization of the trap by the Frenkel effect is given by the expression [16,17]:

$$P = \nu \exp\left(-\frac{W - \left(\frac{e^3}{\pi\varepsilon_\infty\varepsilon_0}\right)^{1/2}}{kT}\sqrt{U/d}\right), \tag{2}$$

where $\nu = W/h$ is the frequency factor, W is the trap energy in the zero field, h — Planck's constant, $e_\infty = n^2 = (1.68)^2 = 2.82$ — high-frequency permittivity, e_0 is the dielectric constant, n is the refractive index, U is the voltage, d is the dielectric thickness, k — Boltzmann constant, T is the temperature.

In the Hill–Adachi model (H–A) overlapping Coulomb traps the probability of trap ionization is described by the expression [18,19]:

$$P = 2\nu \exp\left(-\frac{W - \frac{e^2}{\pi\varepsilon_\infty\varepsilon_0}}{kT}\right)\sinh\left(\frac{e\frac{U}{d}a}{2kT}\right), \tag{3}$$

where a is the average distance between the traps.

According to the Makram-Ebeid and Lannoux model (ME–L), charge transport in a dielectric is described by the ionization of a multiphonon isolated trap. The probability of trap ionization in the ME–L model [20]:

$$P = \sum \exp\left(\frac{nW_{ph}}{2kT} - \frac{W_{opt} - W_t}{W_{ph}}\coth\frac{nW_{ph}}{2kT}\right) \times I_n\left(\frac{W_{opt} - W_t}{W_{ph}\sinh(W_{ph}/2kT)}\right)P_i(W_t + nW_{pt}), \tag{4}$$

$$P_i = \frac{e(U/d)}{2\sqrt{2m^*(W_t + nW_{ph})}}\exp\left(-\frac{4}{3}\frac{\sqrt{2m^*}}{\hbar e(U/d)}(W_t + nW_{ph})^{3/2}\right), \tag{5}$$

where W_t is the thermal energy of the trap, W_{opt} is the optical energy of the trap W_{ph} is the phonon energy, m^* is the effective mass of the electron, I_n is the Bessel function, $\hbar$ is the reduced Planck constant.

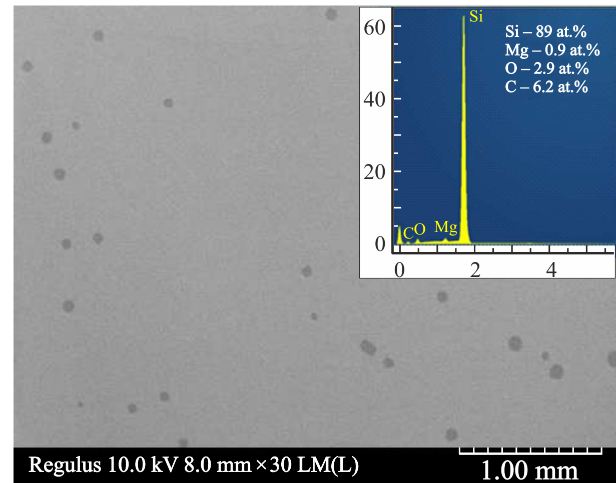

Figure 1. SEM image of the MgO surface and data from energy dispersive X-ray analysis (insert).

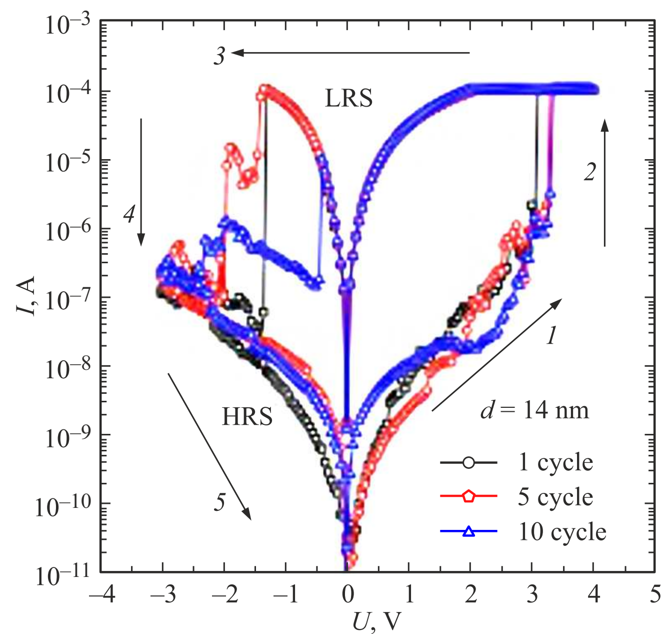

Figure 2. I-V characteristics memristors based on the MgO of the first, fifth and tenth switching cycles. The numbers *1–5* show the voltage sweep sequence.

The probability of trap ionization in the the Nasyrov and Gritsenko (N–G) model of phonon-assisted tunneling between neighboring traps is given by the expression [21]:

$$P = \frac{2\sqrt{\pi}\hbar W_t}{m^* a^2\sqrt{2kT(W_{opt} - W_t)}}\exp\left(-\frac{W_{opt} - W_t}{kT}\right) \times \exp\left(-\frac{2a\sqrt{2m^* W_t}}{\hbar}\right)\sinh\left(\frac{eUa}{2kTd}\right). \tag{6}$$

Variable simulation parameters for different models

State	Frenkel effect	X–A	ME–L	H–G
HRS	$N = 0.35\,\text{cm}^{-3}$ $W = 0.2\,\text{eV}$ $\nu = 4.8 \cdot 10^{13}\,\text{s}^{-1}$ $\varepsilon_0 = 20$	$N = 2 \cdot 10^{20}\,\text{cm}^{-3}$ $W = 0.3\,\text{eV}$ $\nu = 0.95\,\text{s}^{-1}$ $\varepsilon_0 = 20$	$N = 20\,\text{cm}^{-3}$ $m^* = 0.5m_e$ $W_t = 0.15\,\text{eV}$ $W_{opt} = 0.3\,\text{eV}$	$N = 2 \cdot 10^{20}\,\text{cm}^{-3}$ $m^* = 9.6m_e$ $W_t = 0.3\,\text{eV}$ $W_{opt} = 0.6\,\text{eV}$
LRS	$N = 20\,\text{cm}^{-3}$ $W = 0.13\,\text{eV}$ $\nu = 3.1 \cdot 10^{13}\,\text{s}^{-1}$ $\varepsilon_0 = 19$	$N = 6 \cdot 10^{19}\,\text{cm}^{-3}$ $W = 0.2\,\text{eV}$ $\nu = 90\,\text{s}^{-1}$ $\varepsilon_0 = 20$	$N = 5 \cdot 10^{4}\,\text{cm}^{-3}$ $m^* = 0.5m_e$ $W_t = 0.11\,\text{eV}$ $W_{opt} = 0.22\,\text{eV}$ $W_{ph} = 0.06\,\text{eV}$	$N = 6 \cdot 10^{19}\,\text{cm}^{-3}$ $m^* = 4.5m_e$ $W_t = 0.2\,\text{eV}$ $W_{opt} = 0.4\,\text{eV}$

The weak dependence of current on temperature in weak fields, and the absence of temperature dependence in strong fields is not described by the Frenkel effect [16,17], the Hill–Adachi model of overlapping Coulomb trap ionization [18,19], the Makram-Ebeid and Lannoo model of multiphonon isolated trap ionization [20], the Nasyrov and Gritsenko model of phonon-assisted tunneling between neighboring traps [21] (see table).

Such a temperature dependence can be described within the framework of the space charge-limited current model (SCLC) [22]. The I-V characteristics in HRS and LRS can be divided into 3 sections: ohmic, quadratic and exponential. The full expression of the current for such a case is described by the expression [22–24]:

$$I = Se\mu n_f \frac{U}{d} + S\frac{9}{8}\mu\varepsilon\varepsilon_0\theta\frac{U^2}{d^3} + SN_e\mu e^{1-l}\left(\frac{\varepsilon l}{N_c(l+1)}\right)^{l}\left(\frac{2l+1}{l+1}\right)^{l+1}\frac{U^{l+1}}{d^{2l+1}}, \quad (7)$$

where

$$n_f = \frac{2N_d}{1+\sqrt{1+\frac{4gN_d}{N_c}\exp\left(\frac{E_a}{kT}\right)}},$$

$$\theta = \frac{N_c}{N_t}\exp\left(-\frac{W_t}{kt}\right), \quad N_c = 2\left(\frac{2\pi m^* kT}{h^2}\right)^{3/2},$$

where μ is the electron mobility, n_f is the concentration of free electrons in the dielectric, ε is the static permittivity, θ is the degree of filling traps, N_d is the concentration of donor-like defects, g is degeneracy coefficient, N_c is effective density of states, E_a is activation energy of donor-like defects, N_t is trap concentration, $l = T_t/T$, T_t is temperature parameter characterizing the exponential distribution of traps, W_t is trap ionization energy.

As can be seen from formula (7), the SCLC model contains a large number of freely adjustable parameters. The MgO-based memristor is a forming-free memristor. Therefore, the conduction in the HRS of the memristor is carried out over the entire contact area with a radius of $200\,\mu$m, as we did in our other study in Ref. [25]. Based on the fact that the memristor is formless, we make another

Space-charge-limited current
HRS
$N_t = 1.7 \cdot 10^{18}\,\text{cm}^{-3}$
$N_d = 1.5 \cdot 10^{21}\,\text{cm}^{-3}$
$\theta = 1$
$E_a = 0.1\,\text{eV}$
$m^* = 0.5m_e$
$d = 14\,\text{nm}$
$\mu = 8.7 \cdot 10^{-11}\,\text{m}^2/(\text{V}\cdot\text{s})$
$\varepsilon = 9.8$
$l = 26$
$r = 200\,\mu\text{m}$

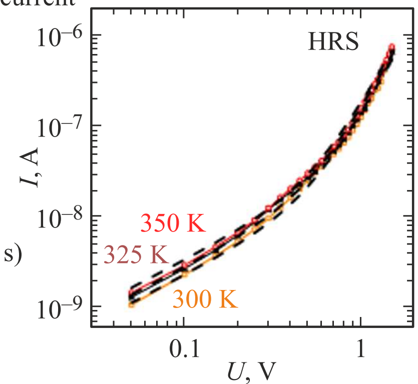

Space-charge-limited current
LRS
$N_t = 0.8 \cdot 10^{18}\,\text{cm}^{-3}$
$N_d = 1.5 \cdot 10^{21}\,\text{cm}^{-3}$
$\theta = 1$
$E_a = 0.09\,\text{eV}$
$m^* = 0.5m_e$
$d = 14\,\text{nm}$
$\mu = 5.1 \cdot 10^{-4}\,\text{m}^2/(\text{V}\cdot\text{s})$
$\varepsilon = 12$
$l = 2.2$
$r = 10\,\text{nm}$

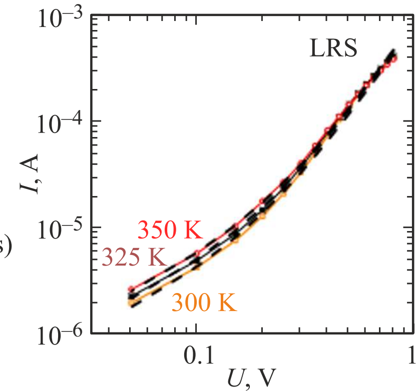

Figure 3. I-V characteristics MgO-based memristors at different temperatures and theoretical curves of the SCLC model for HRS (*a*) and LRS (*b*) memristors. The parameters of the SCLC modeling are shown in figures.

assumption that there is no conductive filament in the HRS and the conductivity goes through the entire MgO layer. In this case, we assume a static dielectric constant of 9.8, as in a conventional dielectric of MgO. The effective mass did not change during the calculations and was assumed to be 0.5.

Taking these assumptions into account, modeling of experimental I-V characteristics in HRS using the SCLC model gives the following parameters: concentration of donor-like defects $N_d = 1.5 \cdot 10^{21}\,\text{cm}^{-3}$, activation energy $E_a = 0.1\,\text{eV}$ and mobility $\mu = 8.7 \cdot 10^{-11}\,\text{cm}^2/(\text{V}\cdot\text{s})$ (Fi-

gure 3, *a*). There is no temperature dependence of the current in the quadratic section. Therefore, the parameter of the degree of filling of traps θ is 1 and it is impossible to determine the concentration of traps from the quadratic area. The concentration of traps is determined from the third section of the experimental curve. The degree of this part is $U^{3.6}$. From the simulation of the third section, the trap concentration is $N_t = 1.7 \cdot 10^{18}\,\mathrm{cm}^{-3}$.

The conducting filament in the LRS, as we believe, is formed due to oxygen deficiency and consists of MgO_x ($x < 1$). The size and composition of the conducting filament MgO_x in LRS are unknown. For the calculation in LRS, we assume a static dielectric constant of 12, and the effective size of the conducting filament is assumed to be a cylinder with a radius of 10 nm. With such values of static permittivity and the effective size of the conducting filament in LRS, the following parameters are obtained when modeling within the framework of the SCLC model: concentration of donor-like defects $N_d = 1.5 \cdot 10^{21}\,\mathrm{cm}^{-3}$, activation energy $E_a = 0.09\,\mathrm{eV}$, mobility $\mu = 5.1 \cdot 10^{-4}\,\mathrm{cm}^2/(\mathrm{V} \cdot \mathrm{s})$ and concentration of traps $N_t = 0.8 \cdot 10^{18}\,\mathrm{cm}^{-3}$ (Figure 3, *b*).

Both HRS and LRS exhibit a weak temperature dependence of the current, but the current still increases with increasing temperature, indicating that the nature of the conductivity in an MgO-based memristor is closer to a semiconductor or dielectric nature than to a metallic one.

Thus, a memristor structure with an active MgO layer was obtained. The MgO-based memristor does not require a forming procedure and has a memory window of about three orders of magnitude. The temperature dependences of the current in the low-resistance and high-resistance states are modeled. The mechanism of charge transport in an MgO-based memritor is described by the space-charge-limited current model. Trap concentrations were determined in the high-resistance ($N_t = 1.7 \cdot 10^{18}\,\mathrm{cm}^{-3}$) and low-resistance ($N_t = 0.8 \cdot 10^{18}\,\mathrm{cm}^{-3}$) states of the MgO-based memristor.

Funding

The study was conducted at the expense of the state assignment of the A.V. Rzhanov Institute of Semiconductor Physics of the Siberian Branch of the Russian Academy of Sciences No. FWGW-2025-0010.

Acknowledgments

The authors are grateful for the opportunity to carry out electrophysical and ellipsometric measurements using the equipment of the Core Facilities VTAN in the Department of the Analytical and Technological Research Center of the NSU.

Conflict of interest

The authors declare that they have no conflict of interest.

References

[1] J. Li, W. Hu, Q. Wei, S. Wu, S. Hua, J. Zhang. J. Electron. Mater. **46**, 1466–1475 (2017).

[2] A. O'Mahony, C.A. Craven, M.J. Minot, M.A. Popecki, J.M. Renaud, D.C. Bennis, J.L. Bond, M.E. Stochaj, M.R. Foley, B.W. Adams, A.U. Mane. J. Vacuum Sci. Techn. A **34**, 01A128 (2016).

[3] Y. Wan, C. Samundsett, J. Bullock, M. Hettick, T. Allen, D. Yan, J. Peng, Y. Wu, J. Cui, A. Javey, A. Cuevas. Adv. Energy Mater. **7**, 1601863 (2017).

[4] F. Schleicher, U. Halisdemir, D. Lacour, M. Gallart, S. Boukari, G. Schmerber, V. Davesne, P. Panissod, D. Halley, H. Majjad, Y. Henry, B. Leconte, A. Boulard, D. Spor, N. Beyer, C. Kieber, E. Sternitzky, O. Cregut, M. Ziegler, F. Montaigne, E. Beaurepaire, P. Gilliot, M. Hehn, M. Bowen. Nat. Commun. **5**, 4547 (2014).

[5] S. Jung, H. Lee, S. Myung, H. Kim, S.K. Yoon, S.-W. Kwon, Y. Ju, M. Kim, W. Yi, S. Han, B. Kwon, B. Seo, K. Lee, G.-H. Koh, K. Lee, Y. Song, C. Choi, D. Ham, S.J. Kim. Nature **601**, 211–216 (2022).

[6] S.C.W. Chow, P.A. Dananjaya, J.M. Ang, D.J.J. Loy, J.R. Thong, S.W. Hoo, E.H. Toh, W.S. Lew. Appl. Surf. Sci. **608**, 55233, (2023). DOI: 10.1016/j.apsusc.2022.155233

[7] J.M. Teixeira, J. Ventura, R. Fermento, J.P. Araujo, J.B. Sousa, P. Wisniowski, P.P. Freitas. J. Phys. D: Appl. Phys. **42**, 105407 (2009).

[8] L.M. Guerra, C. Dias, J. Pereira, H. Lv, S. Cardoso, P.P. Freitas, J. Ventura. J. Nanosci. Nanotechnol. **17**, 564–567 (2017).

[9] W. Lu, W. Chen, Y. Li, R. Jha. IEEE J. Emerging Sel. Top. Circuits Syst. **6**, 163–170 (2016).

[10] L. Yan, C.M. Lopez, R.P. Shrestha, E.A. Irene, A.A. Suvorova, M. Saunders. Appl. Phys. Lett. **88**, 142901, (2006). DOI: 10.1063/1.2191419

[11] A. Posadas, F.J. Walker, C.H. Ahn, T.L. Goodrich, Z. Cai, K.S. Ziemer. Appl. Phys. Lett. **92**, 233511 (2008). DOI: 10.1063/1.2944865

[12] J. Guo, S. Ren, L. Wu, X. Kang, W. Chen, X. Zhao. Appl. Surf. Sci. **434**, 1074–1078 (2018). DOI: 10.1016/j.apsusc.2017.11.026

[13] S.L. Fang, W.H. Liu, X. Li, X.L. Wang, L.i. Geng, M.S. Wu, X.D. Huang, C.Y. Han. Appl. Phys. Lett. **115**, 244102 (2019).

[14] B. Dang, Q. Wu, J. Sun, M. Zhao, S. Wang, F. Song, M. Yang, X. Ma, H. Wang, Y. Hao. IEEE Electron Device Lett. **40**, 1265 (2019).

[15] Y. Cao, S. Wang, J. Lv, F. Li, Q. Liang, M. Yang, X. Ma, H. Wang, Y. Hao. IEEE Trans. Electron Devices **69**, 3118, (2022).

[16] Ya.I. Frenkel'. ZhETF (in Russian) **8**, 1292–1301 (1938).

[17] J. Frenkel. Phys. Rev. B **54**, 647 (1938).

[18] R.M. Hill. Philosophical Magazine **23**, 59–86 (1971).

[19] H. Adachi, Y. Shibata, S. Ono. J. Phys. D: Appl. Phys. **4**, 988–994 (1971).

[20] S.S. Makram-Ebeid, M. Lannoo. Phys. Rev. B **25**, 6406 (1982).

[21] K.A. Nasyrov, V.A. Gritsenko. J. Appl. Phys. **109**, 093705 (2011).

[22] M.A. Lampert, P. Mark. Current injection in solids. Academic Press, N.-Y. (1970). 351 p.

[23] V.A. Voronkovskii, V.S. Allev, A.K. Gerasimova, D.R. Islamov, Mater, Res, Express **6**, *7*, 076411 (2019).
[24] A.A. Gismatulin, G.N. Kamaev, V.N. Kruchinin, V.A. Gritsenko, O.M. Orlov, A. Chin. Sci. Rep. **11**, 2417 (2021). DOI: 10.1038/s41598-021-82159-7
[25] A.A. Gismatulin, O.M. Orlov, V.A. Gritsenko, G.Ya. Krasnikov. Chaos Solitons Fract. **142**, 110458 (2021). DOI: 10.1016/j.chaos.2020.110458

Translated by A.Akhtyamov